Article

Hydroconversion of Waste Cooking Oil into Bio-Jet Fuel over NiMo/SBUY-MCM-41

Zongwei Zhang [1,2], **Qingfa Wang [2,*]** and **Xiangwen Zhang [2,*]**

1   Airport Department Civil Aviation University of China, Tianjin 300300, China; zhv116@163.com
2   Key Laboratory of Green Chemical Technology of Ministry of Education, School of Chemical Engineering
    and Technology, Tianjin University, Tianjin 300072, China
*   Correspondence: qfwang@tju.edu.cn (Q.W.); zhangxiangwen@tju.edu.cn (X.Z.);
    Tel./Fax: +86-22-27892340 (Q.W. and X.Z.)

check for updates

Abstract: A hierarchical SBUY-MCM-41 catalyst was prepared by sacrificing USY (a microporous molecular sieve) to synthesize the MCM-41 zeolite via a hydrothermal method. The hydroconversion of waste cooking oil into hydrocarbon fuel over a NiMo/SBUY-MCM-41 catalyst was investigated. The micropores of the Y building units were inherited by the SBUY-MCM-41 zeolite, in which a special hierarchical structure was formed and the accessibility of reactants to the micropore active sites was improved. The hierarchical SBUY-MCM-41 showed high acidity and hydrothermal stability. Compared with mesoporous Al-MCM-41 and microporous USY zeolites, the SBUY-MCM-41-supported NiMo catalyst significantly enhanced the selective cracking of waste cooking oil for the production of jet-fuel-range hydrocarbons (37.3%), with the highest selectivity for the formation of C_{10}–C_{14} hydrocarbons and a satisfactory selectivity for the formation of jet-fuel-range aromatics (7.6%), as well as a few cyclic compounds. The improved selectivity is the result of the special hierarchical structure and acid distribution of SBUY-MCM-41. This work provides a new strategy to synthesize a hierarchical catalyst for producing alternative jet fuel from waste cooking oil and vegetable oils.

Keywords: waste cooking oil; hydroconversion; bio-jet fuel; MCM-41

1. Introduction

The increasing volume of fossil fuels expended and the resulting carbon emissions continue to exacerbate climate change. In light of this, the production of aviation fuel from renewable energy sources has been extensively studied [1–5]. Accordingly, the hydroconversion of plant oils into bio-jet fuel is a promising strategy to reduce the use of fossil fuels. Haldor Topsoe's HydroFlex™ technology and the UOP (Universal Oil Products Company) Renewable Jet Fuel Process™ were developed to convert plant oil (jatropha oil, animal fats and oils, palm oil, etc.) into bio-jet fuel in two-step processes. Many researchers have also focused on developing a one-step process to obtain bio-jet fuel from plant oils [6–9]. These processes are important for their potential industrial application. Recently, waste cooking oil (WCO) has emerged as a promising feedstock for biofuel production [10–12] because it is 2–3 times cheaper than plant oils [13]. The deoxygenation mechanism and the selectivity for the formation of jet fuel have been the focus of WCO research [14,15].

Screening hydroconversion catalysts to find those with a high selectivity of jet fuel and suitable hydrocarbon formation from WCO is a critical step. Micro-/mesoporous composite hierarchical zeolite has been considered a promising material for such catalysts because it combines the advantages of microporous zeolite's strong acidity and mesoporous zeolite's suitable pores [9,14]. USY zeolite has strong acidity and plentiful micropores and has been widely used as a hydrocracking catalyst. MCM-41

has been extensively applied in catalysis because of its large pore size, which allows the effective diffusion of macromolecules. However, compared with microporous zeolites, MCM-41 has weak acidity and relatively low hydrothermal stability because of the highly amorphous nature of its pore walls. Consequently, significant research efforts have been dedicated to improving the acidity and hydrothermal stability of MCM-41 [16,17].

In this context, zeolite Y building units were used in this work to assemble an MCM-41 structure with increased acidity and hydrothermal stability. The resulting catalyst composed of Ni and Mo supported on the composite hierarchical molecular sieve was used in the hydroconversion of WCO into renewable jet fuel. The aim of using these two materials is to leverage both of their advantages (i.e., enhanced diffusion from the mesoporous material and strong acid sites from USY) to carry out the special reaction. For comparison, pure microporous USY zeolites and pure mesoporous acidic MCM-41 zeolites modified by aluminum were also investigated. The reaction pathways over these catalysts are discussed in this paper. The results could provide an economic route for generating bio-jet fuel from renewable resources and give some insight into the practical design of hierarchical zeolites for the catalytic hydrodeoxygenation of WCO.

2. Results and Discussion

2.1. Textural Structures of Zeolites

Figure 1 shows the X-ray diffraction (XRD) patterns of the zeolites considered in this study. The wide-angle XRD pattern of the SBUY-MCM-41 zeolite (Figure 1b) shows that USY loses its crystal structure and decomposes into secondary building units in an acidic medium. From the low-angle XRD pattern (Figure 1a), two distinct reflections for SBUY-MCM-41 are observed: an intense one at 2.239° and a weak one at 4.2°, which can be indexed to the (100) and (110) planes, respectively [18]. The characteristic peak for Al-MCM-41 is only observed at a higher angle of diffraction (2.4°). This indicates that the unit cell structure of SBUY-MCM-41 is larger than that of Al-MCM-41 because the stiffness and space volume of the secondary USY building units of SBUY-MCM-41 are higher than those of the silicate condensation polymer of Al-MCM-41.
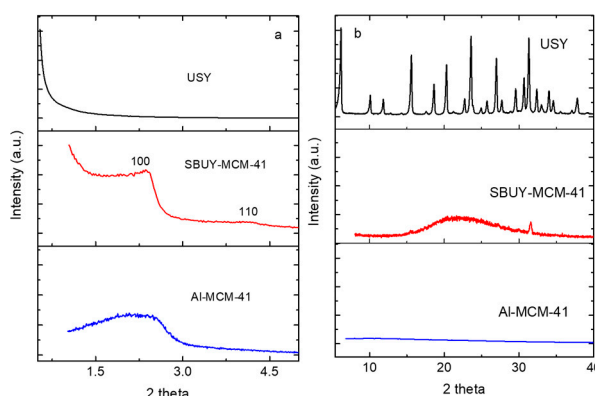
Figure 1. (**a**) Low-angle and (**b**) wide-angle XRD patterns of USY, SBUY-MCM-41, and Al-MCM-41.

The porosity properties of SBUY-MCM-41 and Al-MCM-4 are summarized in Table 1. Table 1 shows that the pore diameter of SBUY-MCM-41 is approximately 2.6 nm, which is smaller than that of Al-MCM-41 (2.8 nm). The wall thickness of SBUY-MCM-41 (1.95 nm) is larger than that of Al-MCM-41 (1.29 nm) owing to the USY secondary building units' larger space volume, which improves the thermal stability of MCM-41 [18,19]. Although the mesopore volume of SBUY-MCM-41 is reduced, the micropore volume of SBUY-MCM-41 (0.06 cm^3 g^{-1}) is considerably increased compared with that of Al-MCM-41 (0 cm^3 g^{-1}). The greater micropore volume improves the accessibility of the reactant to the

active micropore sites and is conducive to the rapid diffusion of the products from the micropores through the mesopores [18].

Table 1. Surface area and pore volume data for Al-MCM-41 and SBUY-MCM-41.

Samples	S_{BET} $(m^2\ g^{-1})$	V_{total} $(cm^3\ g^{-1})$	Unit Cell (nm)	Mesopore Size (nm)	$T_{pore\ wall}$ (nm)
USY	658	0.35	-	-	-
Al-MCM-41	885	0.83	4.09	2.8	1.29
SBUY-MCM-41	820	0.64	4.55	2.6	1.95

V_{total} is the total pore volume at $p/p_0 = 0.99$. $T_{pore\ wall}$ is the thickness of the pore wall.

2.2. Acidity Distributions of Al-MCM-41 and SBUY-MCM-41

The acidity properties of the samples were investigated by ammonia temperature programmed desorption (NH_3-TPD) and Py-FTIR. All the samples presented NH_3 desorption peaks in the ranges of 150–350 °C, 350–450 °C, and 450–550 °C, which are associated with weak, medium, and strong acidity, respectively. The acidity distribution was calculated according to the amounts of desorbed NH_3 and is summarized in Table 2. Table 2 shows that the strong acidity of SBUY-MCM-41 is much higher than that of Al-MCM-41 owing to the contribution of the microstructure of the pore walls in SBUY-MCM-41. The Brønsted/Lewis (B/L) ratio (2.9) of USY is high, indicating that USY is dominated by Brønsted acidity [15]. Compared with USY, SBUY-MCM-41 displays fewer acid sites, especially Brønsted acid sites, because USY was decomposed into secondary building units. The Brønsted acid density of SBUY-MCM-41 is much higher than that of Al-MCM-41, suggesting that the framework Al (the Brønsted acid site) is introduced more easily and with more stability than Al-MCM-41 [18]. The Lewis acidity of SBUY-MCM-41 is also higher than that of Al-MCM-41 because more non-framework Al is formed during the preparation process.

Table 2. Acidity properties of USY, SBUY-MCM-41, and Al-MCM-41 ($\mu mol\ g^{-1}$).

Sample	B	L	B/L	Weak Acidity	Medium Acidity	Strong Acidity
USY	1851	634	2.9	158	530	598
Al-MCM-41	158	212	0.7	78	184	52
SBUY-MCM-41	442	558	0.8	71	224	198

2.3. Reduction Behavior

The hydrogen temperature-programmed reduction (H_2-TPR) results for the different catalysts are shown in Figure 2. The NiMo/USY catalyst shows principal reduction peaks at 505 °C, 572 °C, and 744 °C, which are assigned to the reduction of Mo^{6+} to Mo^{4+} in polymeric octahedral Mo species, the reduction of Ni^{2+} species, and the reduction of tetrahedrally coordinated Mo species in the zeolite cavities, respectively [20,21]. NiMo/SBUY-MCM-41 shows similar reduction behavior, but the peaks are shifted to lower temperatures (481 °C, 540 °C, and 739 °C), indicating an increase in the active phase cluster size [22]. This weakens the active metal–support interaction [22,23]. The peaks of NiMo/Al-MCM-41 are shifted to much lower temperatures (424 °C, 480 °C, and 709 °C). This suggests that there are much weaker interactions between the metal species and the support. Mojet et al. reported that the active metal–support interaction increased as the acidity of the support increased [24]. Table 2 shows that NiMo/Al-MCM-41 has the lowest acidity and that the metal–support interaction is also the weakest, which is in accord with the literatures [24,25].
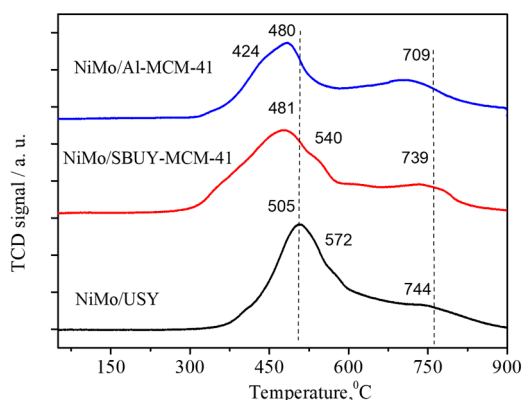
Figure 2. H_2-TPR profiles for NiMo catalysts supported on USY and SBUY-MCM-41.

The CO chemisorption data for the different catalysts are shown in Table 3. The amount of CO adsorbed on NiMo/SBUY-MCM-41 and NiMo/Al-MCM-41 increases dramatically compared with that on NiMo/USY because the specific surface areas of the former two species are higher (Table 1). The amount of adsorbed CO on NiMo/SBUY-MCM-41 is also higher than that on NiMo/Al-MCM-41; this is probably because the latter has a smaller active phase cluster size (Figure 2) [23]. This indicates that the SBUY-MCM-41 support provides better dispersion of the active metals—Ni and Mo—and affords more active sites than the USY and Al-MCM-41 supports.

Table 3. Adsorbed CO determined by TPD characterization.

Sample	Adsorbed CO (μmol g^{-1})
NiMo/USY	1.33
NiMo/Al-MCM-41	3.03
NiMo/SBUY-MCM-41	3.25

2.4. Hydrotreatment of WCO

The hydroconversion of WCO over the three catalysts was also investigated. Approximately 100% conversions were obtained under the given conditions. Figure 3a demonstrates that the organic liquid product (OLP) yield for NiMo/SBUY-MCM-41 reaches 82.1%, which is the highest yield among the three catalysts. This indicates that the use of NiMo/SBUY-MCM-41 does not result in excessive cracking.

There are three reaction pathways for the conversion of triglycerides into alkanes: hydrodeoxygenation (HDO), decarboxylation (DCO_2), and decarbonylation (DCO). In the reported literature and our previous work [8,14,15,26], the C_{17}/C_{18} ratio was used as an index for DCO_x/HDO selectivity. Moreover, the CO_2/CO ratio can be used to distinguish decarboxylation from decarbonylation. For NiMo/USY, the ratio of C_{17}/C_{18} hydrocarbons is 1.60 and the CO_2/CO ratio is 0.17 (Figure 3b). This indicates that DCO_x reactions, especially the DCO reaction, are the primary reaction pathways. For the NiMo/Al-MCM-41 catalyst, the ratio of C_{17}/C_{18} hydrocarbons is much lower (1.0). Furthermore, the NiMo/SBUY-MCM-41 catalyst provides a higher ratio of C_{17}/C_{18} hydrocarbons (1.1) and the highest CO_2/CO ratio (1.21), indicating that the DCO_2 reaction dominates the hydrodeoxygenation process. It has been reported that high acidity favors DCO_x reactions [27,28]. Table 2 shows that the acid density decreases gradually in the order USY > SBUY-MCM-41 > Al-MCM-41. Therefore, the activity for DCO_x reactions over these catalysts decreases in the same order (Figure 3). However, the selectivity of DCO_2 behaved differently over these catalysts. The as-synthesized hierarchical SBUY-MCM-41 is more favorable for carrying out hydrodeoxygenation via the DCO_2 reaction.
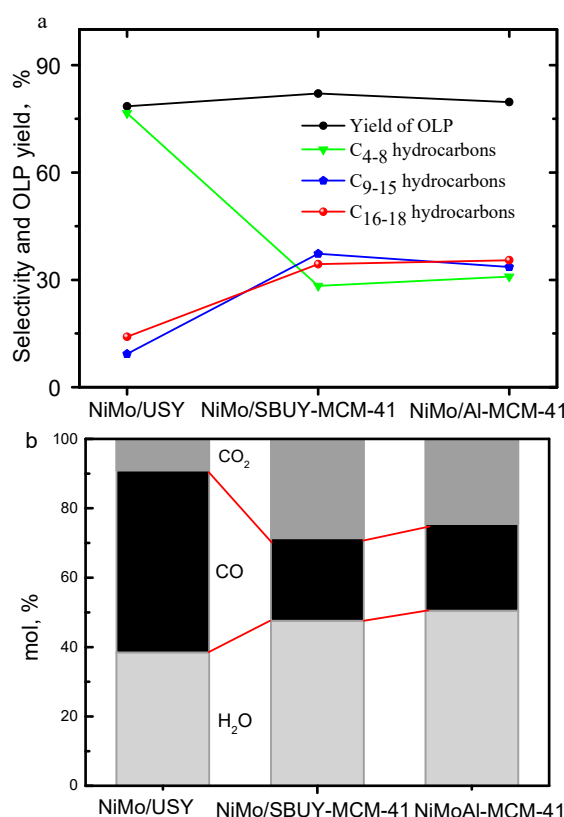
**Figure 3.** (**a**) Hydrocarbon distribution and (**b**) distribution of H_2O, CO, and CO_2 products over different catalysts. Reaction conditions: 380 °C, 3 MPa, 500 mL/mL.

Different distributions of alkanes were formed via selective hydrocracking over the bifunctional catalysts. C_{9-15} hydrocarbons and C_{16-18} hydrocarbons represent jet fuel and diesel fractions, respectively. The gasoline fraction (C_{4-8} hydrocarbons) dominates the products obtained with the NiMo/USY catalyst because of the high values of the medium/strong acidity of the support (Table 2). The Al-MCM-41 zeolite exhibits the lowest values of medium/strong acidity; thus, deep cracking is inhibited, which leads to an increased selectivity for the formation of jet fuel (33.6%). Although the medium/strong acidity and Brønsted acid values of the SBUY-MCM-41 support are higher than those of Al-MCM-41, the selectivity of SBUY-MCM-41 for the formation of C_{9-15} hydrocarbons is significantly increased (up to 37.3%), and its selectivity for the formation of C_{4-8} hydrocarbons is further restricted (to 28.3%). These results indicate that SBUY-MCM-41 significantly enhances the selective cracking to jet-fuel-range hydrocarbons. This is probably because the hierarchical porous structure improves the accessibility of the reactant to the active micropore sites and increases the diffusion of the products from the micropores through the mesopores.

Figure 4 shows the product distributions of C_9–C_{15} hydrocarbons (jet-fuel fraction) produced over different catalysts. Of the three catalysts shown in Figure 4a, NiMo/SBUY-MCM-41 has the highest selectivity for the formation of C_{10}–C_{14}, the optimal jet-fuel fraction. NiMo/USY exhibits the highest selectivity for the formation of aromatic hydrocarbons (29.8%). The hydrocarbon distributions and aromatic selectivity of NiMo/Al-MCM-41 are similar to those of NiMo/SBUY-MCM-41. However, some cyclic compounds (the ideal jet-fuel fraction) and more useable aromatic content are obtained over the NiMo/SBUY-MCM-41 catalyst. Chen et al. [8] reported that cracking reactions (olefins formed), Diels–Alder cyclization reactions (cycloalkanes formed), and dehydrogenation–aromatization (aromatics formed) occur at Brønsted acid sites, Lewis acid sites, and Brønsted acid sites, respectively. They also concluded that the formation of aromatics is jointly influenced by Brønsted and Lewis acidity [8]. The selectivity for the formation of aromatics and cycloalkanes over the Al-MCM-41

catalyst is the lowest, and it is probably because it has the fewest Brønsted acid sites (158 µmol g^{-1}) and the lowest B/L value (0.7). In addition, the density of strong acid sites in Al-MCM-41 is the lowest (52 µmol g^{-1}), which is not beneficial to the dealkylation of the higher aromatics into jet fuel [29]. USY exhibits the highest yield of aromatics because it has the highest density of Brønsted acid sites (1851 µmol g^{-1}) and the highest B/L value (2.9). The SBUY-MCM-41 catalyst has a higher and more satisfactory selectivity for the formation of aromatics because of its moderate density of Brønsted acid sites (442 µmol g^{-1}), suitable B/L value (0.8), and moderate density of strong acid sites (198 µmol g^{-1}).
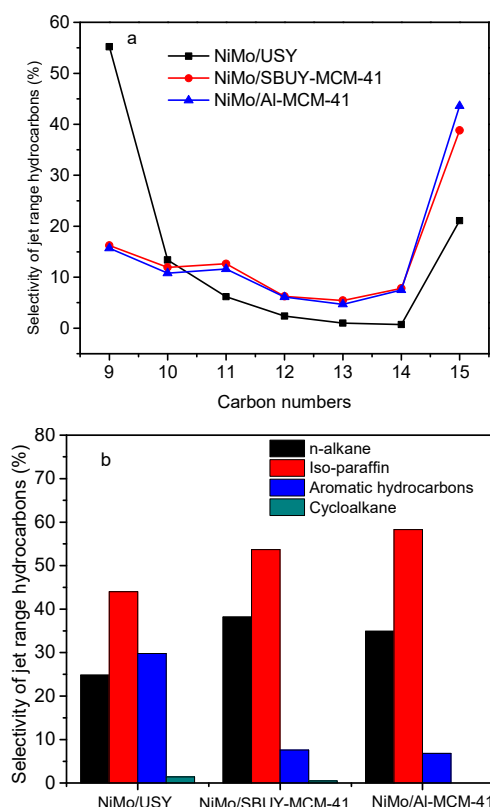
Figure 4. (**a**) Selectivity for the formation of hydrocarbons with different carbon numbers over different catalysts. (**b**) Selectivity for the formation of various jet-fuel-range hydrocarbons using different catalysts. Reaction conditions: 380 °C, 3 MPa, 500 mL/mL.

From the above discussion, the SBUY-MCM-41 structure appears to benefit from both USY and MCM-41. Cracking products escape quickly from MCM-41 with weak acidity and avoid being cracked excessively. Then, the small cracking products form cycloalkanes and aromatics on the dealuminated Y building units with strong acidity, and the higher cycloalkanes and aromatics compose the jet fuel fraction.

Figure 5 shows the variation in product distribution of the C$_{9-15}$ hydrocarbons (jet-fuel fraction) *vs.* time on stream. The iso-/n-paraffin ratio (i/n) and the selectivity for the formation of aromatics decrease slightly with time because the acid sites become covered by basic nitrogen compounds (such as dimethylamine, which is formed after the deterioration of oil and the condiments added to oil during cooking).
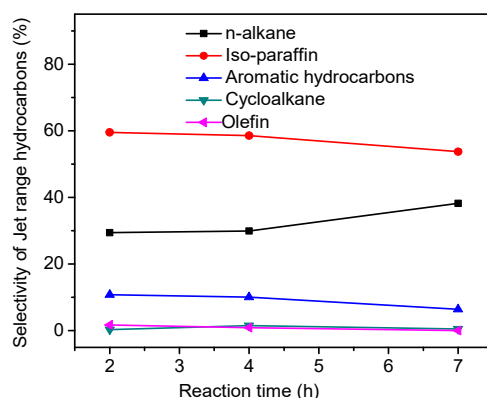
Figure 5. Selectivity for the formation of various jet-fuel-range hydrocarbons in the conversion of WCO over NiMo/SBUY-MCM-41. Reaction conditions: 380 °C, 3 MPa, 500 mL/mL.

2.5. Effects of Temperature, Pressure, and Hydrogen-to-Oil Ratio on the Hydrotreatment of WCO
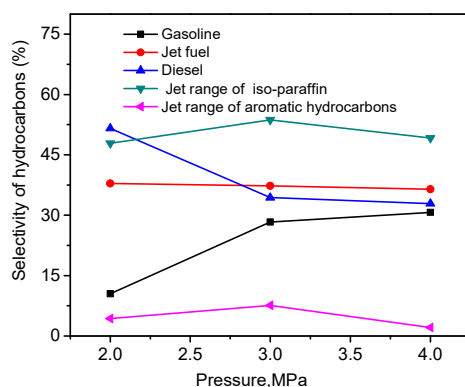
The effect of temperature on hydrocracking performance is shown in Figure 6. The WCO conversions are 90%, 100%, and 100% at 340, 380, and 400 °C, respectively, and the yields of OLPs are very similar to one another (82.9%, 82.1%, and 80.2%). The selectivity for the formation of gasoline products dramatically increases with the decrease in diesel and jet-fuel selectivity because the cracking is enhanced at high temperatures. The selectivity for the formation of iso-paraffin decreases because the reaction is exothermic, and the selectivity for the formation of jet-fuel-range aromatics also decreases with increasing temperature. Thus, an optimal temperature of 380 °C is obtained for jet-fuel selectivity and properties.
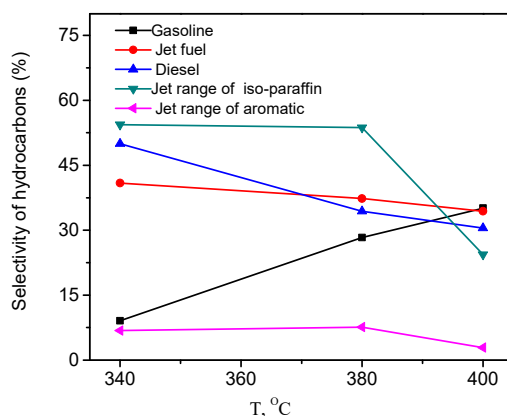
Figure 6. Selectivity for the formation of hydrocarbons using NiMo/SBUY-MCM-41 at different reaction temperatures. Reaction conditions: 3 MPa and 500 mL/mL.

The influence of pressures (ranging from 2 to 4 MPa) on the hydroconversion of WCO was also investigated (Figure 7), and 100% WCO conversions are achieved under these conditions. The yields of OLPs gradually decrease as the pressure increases (83.9%, 82.1%, and 79.2% at 2, 3, and 4 MPa, respectively). Furthermore, as the pressure increases, the selectivity for the formation of gasoline products increases and the selectivity for the formation of diesel decreases. The selectivity for the formation of jet fuel and iso-paraffin varies little with pressure. Low pressure favors the formation of aromatics because it promotes cycloalkane dehydrogenation.

Figure 7. Selectivity for the formation of hydrocarbons using NiMo/SBUY-MCM-41 at different pressures. Reaction conditions: 380 °C, 500 mL/mL.

The effect of the H_2/oil ratio on hydrocracking performance is shown in Figure 8. Approximately 100% WCO conversion is achieved under these conditions. The yields of OLPs at H_2/oil ratios of 250, 500, and 750 are 82.5%, 82.1%, and 78.0%, respectively. As the H_2/oil ratio increases, the selectivity for the formation of jet fuel and iso-paraffin increases and then decreases, with an optimum value at an H_2/oil ratio of 500 mL mL^{-1}. A low H_2/oil ratio favors the formation of aromatics. A likely reason for this is that low H_2/oil ratios promote the dehydrogenation of alkanes and cycloalkanes.
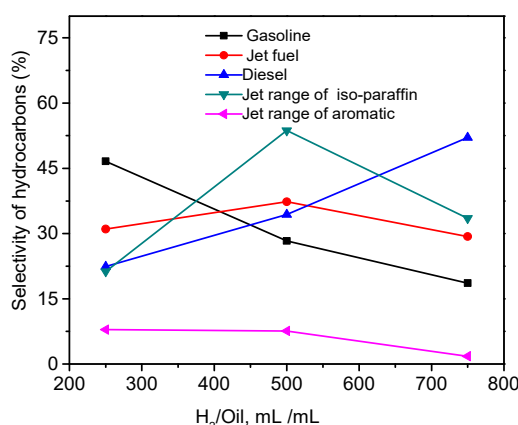

Figure 8. Selectivity for the formation of hydrocarbons using NiMo/SBUY-MCM-41 at different H_2/Oil ratios. Reaction conditions: 380 °C, 3 MPa.

2.6. The Effects of USY Content on the Hydrotreatment of WCO

Figure 9 shows the variation in the product distribution and jet-fuel composition as the USY content changes. The $Na_2SiO_2 \cdot 9H_2O$/USY mass ratios of 11 NiMo/SBUY-MCM-41, NiMo/SBUY-MCM-41, and 4 NiMo/SBUY-MCM-41 are 11, 7, and 4. Figure 9 reveals that the selectivity for the formation of jet fuel varies little with the USY content. However, the selectivity for iso-paraffin decreases with the increase in USY content owing to the higher density of strong acid sites [30] from the secondary Y building units in the pore walls. The selectivity for the formation of cycloalkane increases, and the selectivity for the formation of aromatics increases and then decreases as the USY content increases. Thus, the content of USY has little influence on the hydrocarbon distribution, but it affects the hydrocarbon composition significantly. Therefore, the USY content could be used to adjust product properties.
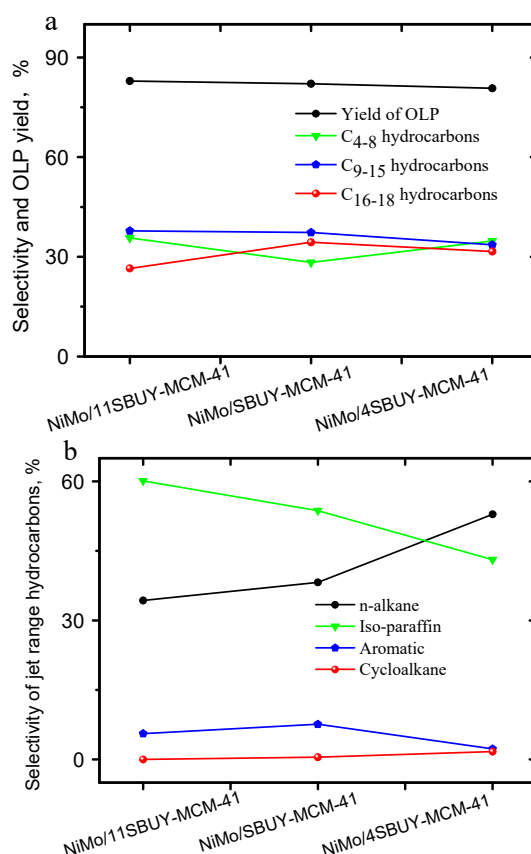
Figure 9. Product selectivity in the hydrotreatment of WCO over NiMo/SBUY-MCM-41. (**a**) Hydrocarbon distribution and (**b**) hydrocarbon composition.

3. Experimental

3.1. Materials

Commercial USY zeolite (Si/Al$_{XRD}$ = 4.1, Si/Al$_{XRF}$ = 8.8) was provided by Nankai University Catalyst Co. (Tianjin, China), $(NH_4)_6Mo_7O_{24}$ (≥99 wt %, J&K Chemical Ltd., Beijing, China), sodium hydroxide (NaOH), sodium silicate, and cyclohexane were supplied by Tianjin Guangfu Chemical Industry (Tianjin, China). WCO was purchased from Tianjin Bihai Environmental Protection Ltd., Co., (Tianjin, China). The WCO used in this study contains a mixture of spent cooking oil and was mainly gathered from local restaurants, after which it was filtered by a regular sieve to remove the remaining food particles before it was used as feedstock. Table 4 lists the main physical and chemical properties.

Table 4. Chemical and physical properties of waste cooking oil.

Property	Waste Cooking Oil
Acid value (mg KOH^{-1})	65.47
Palmitic acid ($C_{16:0}$, wt %)	25.02
Linoleic acid ($C_{18:2}$, wt %)	28.85
Oleic acid ($C_{18:1}$, wt %)	39.69
Stearic acid ($C_{18:0}$, wt %)	6.27
Other acid (wt %)	0.17

3.2. Catalyst Preparation

NiMo/SBUY-MCM-41 preparation: In a typical run [31], the cationic surfactant CTAB (10.934 g) was dissolved in 150 mL of water containing 25 mL of HCl (10 M), and the resulting mixture was added

to a solution containing 42.64 g of $Na_2SiO_3 \cdot 9H_2O$ and 6 g of USY in 150 mL of water. The mixture was stirred for 0.5 h, and then the pH was adjusted to 1.0. The mixture was transferred to an autoclave for further condensation at a hydrothermal crystallization temperature of 120 °C for one day after stirring at room temperature for 2 h. Next, the catalyst was dried at 120 °C for 12 h and then converted into an H-type catalyst by three ion-exchange processes (10 g of sample in 100 mL of 0.5 M NH_4NO_3). Ni (4.0 wt %) and Mo (12 wt %) were loaded onto the hierarchical USY by incipient wetness co-impregnation using aqueous $Ni(NO_3)_2$ and $(NH_4)_6Mo_7O_{24}$. Then, the samples were stored overnight at room temperature, dried at 120 °C for 12 h, and calcinated at 550 °C for 5 h. The obtained catalyst was designated NiMo/SBUY-MCM-41.

NiMo/Al-MCM-41 preparation: The above procedure was repeated without adding USY to obtain MCM-41. Then, 4 g of the calcinated sample was further modified with 0.68 g of aluminum isopropoxide in 160 mL of 0.03 M HCl solution. The drying, calcination, and Ni/Mo impregnation were performed as above to obtain NiMo/Al-MCM-41.

3.3. Characterizations

XRD testing was conducted using a D/MAX-2500 X-ray diffractometer (Tokyo, Japan) with (Cu-Kα) radiation at 40 kV and 140 mA. The zeolites were measured in the 2θ range from 0° to 10° and from 5° to 60°, respectively.

A chemisorption physisorption analyzer (AMI-300, Altamira Instruments, Pittsburgh, PA, USA) equipped with a thermal conductivity detector (TCD) was used to measure ammonia temperature programmed desorption (NH_3-TPD). After pretreatment at 500 °C in He for 1 h, the samples were cooled to 80 °C, and NH_3 adsorption was then carried out by NH_3 in He at 120 °C for 30 min. After removing weakly adsorbed NH_3 by blowing with He at 393 K for 2 h, the NH_3-TPD profile was recorded from 120 °C to 700 °C.

The AMI-300 was also used to conduct H_2-TPR experiments. After pretreatment at 450 °C in He for 1 h, the samples were cooled to ambient temperature before measurement. A mixture of 10% H_2 + 90% He was heated at a heating rate of 10 °C/min up to 900 °C in the reduction step. For CO chemisorption, after being pretreated in helium at 120 °C for 1 h, the sample (100 mg) was reduced in H_2 flow (50 cm^3/min) at 450 °C for 2 h and then evacuated at 450 °C for 2 h. Afterward, the sample was cooled to 40 °C under vacuum, and then the CO adsorption isotherm was recorded.

A Bruker Vertex 70 FTIR spectrometer (Karlsruhe, Baden-Württemberg, Germany) with a resolution of 4 cm^{-1} was used for Py-FTIR measurements. The sample (10 mg) was pretreated under vacuum at 400 °C for 1 h and then cooled to 200 °C to record the background prior to adsorption experiments. Pyridine was injected into the cell and kept for 30 min in flowing N_2. Then, the spectra were recorded between 1300 and 4000 cm^{-1}.

The pore volumes, pore size distribution, and specific surface areas of the samples were measured by N_2 adsorption–desorption isotherms on a Micromeritics ASAP-2020 apparatus (Atlanta, GA, USA). Before analysis, all samples were pretreated under vacuum at 300 °C for 4 h.

3.4. Hydrotreating of Waste Cooking Oil

The hydroconversion of WCO was carried out in a fixed-bed flow reactor (1.2 cm I.D. and 45 cm in length). The reaction temperature range (from 340 °C to 400 °C) was dominated by four thermocouples on the reactor wall and controlled by a thermocouple in the catalyst bed. Hydrogen was supplied at a rate that ranged from 12 L/h to 36 L/h under an experimental pressure range of 2–4 MPa. SiC was used to dilute 8 g of the catalyst to obtain a sufficient catalyst-bed length, and the catalyst was then loaded into the steel reactor. WCO (20 wt %) in cyclohexane was used as the feedstock and supplied at a flow rate of 0.8 mL/ min. The H_2/oil ratio was determined by the hydrogen flow and the total liquid feed flow. The fundamental reactions were conducted at 380 °C and 3 MPa with an H_2/oil ratio (mL/mL) of 500. The catalysts were presulfided in situ at 320 °C and 3.0 MPa for 4 h using 3.0 wt % CS_2 in cyclohexane.

The products were collected and separated into gaseous products, liquid products (OLPs), and water after the reaction reached stability (at least 5 h). The gaseous products were determined with an Agilent Micro 3000 gas chromatograph equipped with three columns (molecular sieve, plot U, and alumina) and TCD detectors. The organic liquid products were qualitatively analyzed with an Agilent 6890N gas chromatography/5975N mass spectrometry (GC/MS) and quantitatively analyzed using a gas chromatographs (Bruker 456 GC, Bruker, San Francisco, CA, USA) equipped with a flame ionization detector (FID) and a commercial column (ZB-5 HT, 60 m × 0.25 mm × 0.25 μm). The water was weighted. The conversion of WCO and the selectivity for the formation of hydrocarbons were calculated by Equations (1)–(3):

$$\text{Conversion} = 100\% \times (\text{Feed}_G - \text{Product}_G)/\text{Feed}_G \qquad (1)$$

$$\text{Selectivity}_{(C_xH_y)} = (CH)_{nproducts}/\Sigma(CH)_{nproducts} \qquad (2)$$

$$\text{Selectivity for the formation of aromatics} = \Sigma(CH)_{aromatics}/\Sigma(CH)_{nproducts} \qquad (3)$$

where Feed_G and products_G represent the weights of WCO in the feed and the products, respectively; $(CH)_{nproducts}$ represents the weight of C_n hydrocarbons in the products.

4. Conclusions

The density of strong acid sites and the hydrothermal stability of the SBUY-MCM-41 zeolite assembled with Y building units were higher than those of Al-MCM-41 prepared by postgrafting with aluminum isopropoxide. The micropores of the Y building units were inherited by the SBUY-MCM-41 zeolite, in which a special hierarchical structure was formed and the accessibility of reactants to the micropore active sites was also improved. NiMo/SBUY-MCM-41 significantly enhanced the selective cracking of waste cooking oil for jet-fuel-range hydrocarbons (37.3%), with the highest selectivity for the formation of C_{10}–C_{14} hydrocarbons and a satisfactory selectivity for the formation of jet-fuel-range aromatics (7.6%) as well as a few cyclic compounds. The improved selectivity is the result of the special hierarchical structure and acid distribution of SBUY-MCM-41. Thus, a new strategy is provided to synthesize a hierarchical catalyst for producing alternative jet fuel from WCO.

Author Contributions: All authors conceived and designed the experiments; Z.Z. performed the experiments; Q.W. and X.Z. analyzed the data; Z.Z. wrote the paper.

Conflicts of Interest: The authors declare no conflicts of interest.

References

1. Gutiérrez-Antonio, C.; Gómez-Castro, F.I.; de Lira-Flores, J.A.; Hernández, S. A review on the production processes of renewable jet fuel. *Renew. Sustain. Energy Rev.* **2017**, *79*, 709–729. [CrossRef]
2. Wang, M.; Chen, M.; Fang, Y.; Tan, T.W. Highly efficient conversion of plant oil to bio-aviation fuel and valuable chemicals by combination of enzymatic transesterification, olefin cross-metathesis, and hydrotreating. *Biotechnol. Biofuels* **2018**, *11*, 30. [CrossRef]
3. Yang, J.; Xin, Z.H.; He, Q.; Corscadden, K.; Niu, H. An overview on performance characteristics of bio-jet fuels. *Fuel* **2019**, *237*, 916–936.
4. Li, Y.P.; Chen, L.G.; Zhang, Q.H.; Zhang, Q.; Wang, T.J.; Qiu, S.B.; Tan, J.; Li, K.; Ma, L.L. Process and techno-economic analysis of bio-jet fuel-range hydrocarbon production from lignocellulosic biomass via aqueous phase deconstruction and catalytic conversion. *Energy Procedia* **2017**, *105*, 675–680. [CrossRef]
5. Ju, C.; Wang, M.; Huang, Y.; Fang, Y.; Tan, T.W. High-quality jet fuel blend production by oxygen-containing terpenoids hydroprocessing. *ACS Sustain. Chem. Eng.* **2018**, *6*, 4871–4879. [CrossRef]
6. Zhou, W.J.; Xin, H.; Yang, H.R.; Du, X.Z.; Yang, R.; Li, D.; Hu, C.W. The Deoxygenation Pathways of Palmitic Acid into Hydrocarbons on Silica-Supported $Ni_{12}P_5$ and Ni_2P Catalysts. *Catalysts* **2018**, *8*, 153. [CrossRef]

7. Zhang, C.F.; Chen, H.; Zhang, X.W.; Wang, Q.F. TPABr-grafted MWCNT as bifunctional template to synthesize hierarchical ZSM-5 zeolite. *Mater. Lett.* **2017**, *197*, 111–114. [CrossRef]

8. Chen, H.; Wang, Q.F.; Zhang, X.W.; Wang, L. Quantitative conversion of triglycerides to hydrocarbons over hierarchical ZSM-5 catalyst. *Appl. Catal. B Environ.* **2015**, *166–167*, 327–334. [CrossRef]

9. Li, T.; Cheng, J.; Huang, R.; Zhou, J.; Cen, K. Conversion of waste cooking oil to jet biofuel with nickel-based mesoporous zeolite Y catalys. *Bioresour. Technol.* **2015**, *197*, 289–294. [CrossRef]

10. Bezergianni, S.; Voutetakls, S.; Kalogianni, A. Catalytic hydrocracking of fresh and used cooking oil. *Ind. Eng. Chem. Res.* **2009**, *48*, 8402–8406. [CrossRef]

11. Talebian-Kiakalaieha, A.; Amina, N.A.S.; Mazaheria, H. A review on novel processes of biodiesel production from waste cooking oil. *Appl. Energy* **2013**, *104*, 683–710. [CrossRef]

12. Morais, S.; Mata, T.M.; Martins, A.A.; Pinto, G.A.; Costa, C.A.V. Simulation and life cycle assessment of process design alternatives for biodiesel production from waste vegetable oils. *J. Clean. Prod.* **2010**, *18*, 1251–1259. [CrossRef]

13. Verma, D.; Rana, B.S.; Kumar, R.; Sibi, M.G.; Sinha, A.K. Diesel and aviation kerosene with desired aromatics from hydroprocessing of jatropha oil over hydrogenation catalysts supported on hierarchical mesoporous SAPO-11. *Appl. Catal. A Gen.* **2015**, *490*, 108–116. [CrossRef]

14. Zhang, Z.Z.; Wang, Q.F.; Chen, H.; Zhang, X.W. Hydroconversion of waste cooking oil into biojet fuel over hierarchical NiMo/USY@Al-SBA-15 zeolite. *Chem. Eng. Technol.* **2018**, *41*, 590–597. [CrossRef]

15. Zhang, Z.Z.; Wang, Q.F.; Chen, H.; Zhang, X.W. Hydroconversion of waste cooking oil into green biofuel over hierarchical USY supported NiMo catalyst a comparative study of desilication and dealumination. *Catalysts* **2017**, *7*, 281. [CrossRef]

16. Li, P.; Liu, L.P.; Xiong, G. Effect of zeolite precursor on the formation of MCM-41 molecular sieve containing zeolite Y building units. *Phys. Chem. Chem. Phys.* **2011**, *13*, 11248–11253. [CrossRef]

17. Li, P.; Xiong, G.; Liu, L.P.; Wang, L.L. Investigation on the effect of zeolite precursor on the formation process of MCM-41 containing zeolite Y building units. *Spectrochim. Acta Part A Mol. Biomol. Spectrosc.* **2013**, *107*, 218–226. [CrossRef]

18. Shi, G.; Tan, Q.F.; Liu, H.Y.; Bao, X.J. Templated Assembly of Nano-Crystals of Zeolite Y under Basic Conditions. *Chem. React. Eng. Technol.* **2013**, *29*, 470–480.

19. Han, Y.; Wu, S.; Sun, Y.Y.; Li, D.S.; Xiao, F.S. Hydrothermally stable ordered hexagonal mesoporous aluminosilicates assembled from a triblock copolymer and preformed aluminosilicate precursors in strongly acidic media. *Chem. Mater.* **2002**, *14*, 1144–1148. [CrossRef]

20. Cordero, R.L.; Agudo, A.L. Effect of water extraction on the surface properties of Mo/Al_2O_3 and $NiMo/Al_2O_3$ hydrotreating catalysts. *Appl. Catal. A Gen.* **2000**, *202*, 23–35. [CrossRef]

21. Solís, D.A.; Agudo, L.; Ramírez, J.; Klimova, T. Hydrodesulfurization of hindered dibenzothiophenes on bifunctional NiMo catalysts supported on zeolite–alumina composites. *Catal. Today* **2006**, *116*, 469–477. [CrossRef]

22. Kubička, D.; Horáček, J.; Setnička, M.; Bulánek, R.; Zukal, A.; Kubičková, I. Effect of support-active phase interactions on the catalyst activity and selectivity in deoxygenation of triglycerides. *Appl. Catal. B* **2014**, *145*, 101–107. [CrossRef]

23. Chen, H.; Wang, Q.F.; Zhang, X.W.; Wang, L. Hydroconversion of Jatropha Oil to Alternative Fuel over Hierarchical ZSM-5. *Ind. Eng. Chem. Res.* **2014**, *53*, 19916–19924. [CrossRef]

24. Mojet, B.L.; Miller, J.T.; Ramaker, D.E.; Koningsberger, D.C. A new model describing the metal-support interaction in noble metal catalysts. *J. Catal.* **1999**, *186*, 373–386. [CrossRef]

25. Rajagopal, S.; Marini, H.J.; Marzari, J.A.; Miranda, R. Silica-Alumina-Supported Acidic Molybdenum Catalysts-TPR and XRD Characterization. *J. Catal.* **1994**, *147*, 417–428. [CrossRef]

26. Yang, Y.H.; Wang, Q.F.; Zhang, X.W.; Wang, L.; Li, G.Z. Hydrotreating of C_{18} fatty acids to hydrocarbons on sulphided NiW/SiO_2—Al_2O_3. *Fuel Process Technol.* **2013**, *116*, 165–174. [CrossRef]

27. Gong, S.; Shinozaki, A.; Qian, E.W. Role of Support in Hydrotreatment of Jatropha Oil over Sulfided NiMo Catalysts. *Ind. Eng. Chem. Res.* **2012**, *51*, 13953–13960. [CrossRef]

28. Zhao, Y.; Liu, Z.; Li, W.; Zhao, Y.; Pan, H.; Liu, Y.; Li, M.; Kong, L. Synthesis, characterization, and catalytic performance of high-silica Y zeolites with different crystallite size. *Microporous Mesoporous Mater.* **2013**, *167*, 102–108. [CrossRef]

29. Adjaye, J.D.; Katikaneni, S.P.R.; Bakhshi, N.N. Catalytic conversion of a biofuel to hydrocarbons: Effect of mixtures of HZSM-5 and silica-alumina catalysts on product distribution. *Fuel Process. Technol.* **1996**, *48*, 115–143. [CrossRef]

30. Iliopoulou, E.F.; Heracleous, E.; Delimitis, A.; Lappas, A.A. Producing high quality biofuels: Pt-based hydroisomerization catalysts evaluated using BtL-naphtha surrogates. *Appl. Catal. B Environ.* **2014**, *145*, 177–186. [CrossRef]

31. Wang, Y.; Cui, D.M.; Li, Q.Z. Synthesis, characterization and influence parameters on the overgrowth of micro/mesoporous Y-zeolite-MCM-41 composite material under acidic conditions. *Microporous Mesoporous Mater.* **2011**, *142*, 503–510. [CrossRef]